

Competition for resources in an exclusion model with biased lane-changing mechanism

Ankita Gupta^{✉*} and Arvind Kumar Gupta^{✉†}

Department of Mathematics, Indian Institute of Technology Ropar, Rupnagar-140001, Punjab, India



(Received 11 January 2024; accepted 11 March 2024; published 26 March 2024)

The motivation for the proposed work is drawn from the attachment-detachment observed in biological and physical transport processes that entail finite resources. We investigate the influence of limited particle availability on particle dynamics within two parallel totally asymmetric simple exclusion lanes, with one lane incorporating only particle detachment and the other considering particle attachment. We establish a theoretical framework by employing vertical mean-field theory in conjunction with singular perturbation technique. The analytical findings are supported by numerical and stochastic validation using a finite-difference scheme and the Gillespie algorithm. By utilizing these approaches, we scrutinize various stationary properties, including particle densities, phase boundaries, and particle currents for both lanes. Our analysis reveals that the complexity of the phase diagram exhibits a nonmonotonic trend in the number of stationary phases as the particle count increases. Each phase diagram is constructed with respect to the intrinsic boundary parameters, illustrating both bulk and surface transitions occurring within the lanes. The interplay between finite resources and coupling mechanisms gives rise to two phases involving upward shock in one of the lanes, while two phases exhibit synchronized downward shock in both lanes. Finally, we delve into shock dynamics to comprehend critical phase transitions occurring in the system.

DOI: [10.1103/PhysRevE.109.034132](https://doi.org/10.1103/PhysRevE.109.034132)

I. INTRODUCTION

Most natural occurrences and human-created transport systems commonly undergo evolution in a nonequilibrium state, displaying unique characteristics due to the continuous input of internal or external energy. In recent decades, there has been significant interest in studying such systems across various fields like biology, physics, chemistry, and specific applications such as vehicular flow, ant trails, intracellular transport, gel electrophoresis, and protein synthesis [1–8]. Nonequilibrium states are marked by a nonzero particle current even in a stationary state, posing challenges in developing a comprehensive framework. MacDonald and Gibbs introduced the totally asymmetric simple exclusion process (TASEP) in 1968 to understand nonequilibrium stochastic transport systems, focusing on the kinetics of biopolymerization [9,10]. This model explores the collective dynamics of active particles moving in a preferred direction within a lattice, adhering to the exclusion principle. The lattice can be incorporated with various boundary conditions such as open or periodic boundaries. The open boundaries result in three steady-state phases: low density (LD), high density (HD), and maximal current (MC), which are governed by the entry and exit rate of particles from the extreme ends of the lattice [11–13]. When particle density, functions as an order parameter, a first-order transition occurs from the LD to HD phase, while a second-order transition occurs from either the LD or HD phases to the MC phase. The model, along

with its variants, effectively explains various nonequilibrium phenomena like localized shock formation, phase transitions, symmetry-breaking, and more [11–19].

Over the past few decades, there has been a noticeable increase in the inclination to extend single-dimensional models to coupled multilane systems, motivated by various real-world phenomena. In both vehicular traffic and biological transport, particles demonstrate the capability to adhere to or deviate from their prescribed routes in various systems [20,21]. Several instances from vehicular traffic illustrate such scenarios; a few of them are as follows: (i) Accelerating on the entrance ramp, the driver seamlessly merges into highway traffic by changing lanes, skillfully finding a safe gap in the flow [22]; (ii) when faced with lane closure due to construction, drivers employ zipper merging, alternately merging from closing lanes into open ones; and (iii) faced with an obstacle or hazard in their current lane, drivers swiftly change lanes to steer clear of the impediment, be it road debris or a stalled vehicle [23]. Similarly, in biological transport, motor proteins can attach and detach from microtubules and cytoplasm, allowing for adaptability in their pathways [24]. Another example is seen in ants who optimize resource collection by metaphorically changing lanes on foraging trails, and adjust pheromone-guided paths based on the availability of food sources [25]. In both cases, the ability of particles to switch paths is influenced by the dynamic conditions they encounter.

In light of all these situations, numerous efforts have been made to adapt the exclusion model and explore particle dynamics, considering the particle configuration in neighboring lanes as a significant factor. A theoretical framework employing vertical cluster mean field is employed to analyze a two-channel model with symmetric and asymmetric coupling

*gupta.ankita1995@gmail.com

†akgupta@iitrpr.ac.in

[26,27] or a combination of both [28–31]. The research findings indicate that robust asymmetric coupling results in seven stationary phases, the majority of which exhibit zero particle flux in one of the channels. However, under strong asymmetric coupling, the characteristics of the two lanes become nearly identical. Subsequently, various adaptations of the coupling model were introduced, integrating diverse dynamical rules, including coupling on antiparallel lanes [32,33], multichannel coupled system [34,35], periodic boundaries [36], and Langmuir kinetics [37–43]. Some of them also conducted a thorough examination of the system's stationary properties through a boundary-layer analysis [41–43]. In addition to these studies, some other cellular automata models has been applied to simulate realistic traffic flow scenarios, including multilane systems with and without lane-changing feature [44–48].

Most of the existing literature involves utilizing the open TASEPs to investigate the collective behavior of particles on a lattice equipped with an unrestricted reservoir. In adherence to this approach, the entrance and exit rates remain consistent, regardless of the reservoir's occupancy. However, this may not accurately depict reality. Numerous real-world occurrences, both in the physical and biological realms, such as protein synthesis, motor protein movement, pedestrian flow, and vehicular traffic, entail competition for finite resources within single or multilane systems. In this direction, various versions of the exclusion model have arisen that preserve the total particle count in the system [49], demonstrating a widespread constraint on resources in almost all physical and biological systems [50–53]. Such a restriction leads to a nontrivial effect on the stationary properties resulting in the emergence of a region featuring a delocalized domain wall, referred to as the shock (S) phase. This phase connects a section with a low-density profile on the left to a region with high particle density on the right.

Despite the considerable research devoted to biased lane-changing mechanisms in the multilane exclusion model, there remains a notable gap in the literature regarding studies focused on limited particle resources. Our objective is to establish a theoretical framework for the system and explore the influence of restricted particle resources on stationary properties, while also characterizing its fundamental features. We employ the concept of boundary-layer analysis to derive a comprehensive solution for the density profiles as well as the phase boundaries. These findings are then employed to construct a phase diagram that elucidates both bulk and surface transitions. The present research distinguishes itself from previous investigations in several ways. (i) A global constraint on particle resources is introduced. (ii) Lane changing takes precedence over forward movement, with the former being a certain event. This means that the lane-changing mechanism is biased towards a specific lane. (iii) We provide explicit theoretical expressions for the stationary properties of the system. (iv) Validation of the results is carried out through numerical and stochastic approaches, utilizing finite-difference methods and simulations. (v) Finally, boundary-layer analysis is also performed.

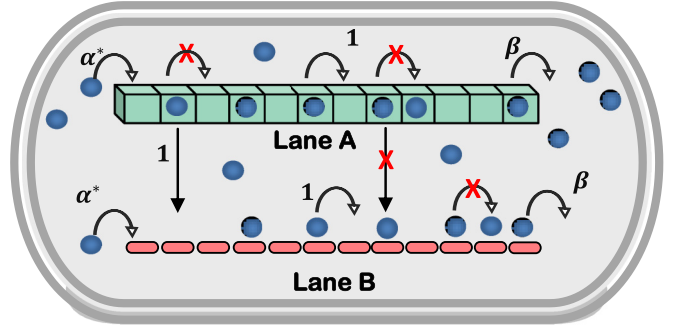


FIG. 1. Illustration of the two-lane exclusion model with open boundaries. Lane A functions as a feeder lane, while lane B serves as an absorber lane. Arrows represent permissible transitions, while crosses indicate restricted transitions. The variables α and β represent the entry and exit rates, respectively.

II. DESCRIPTION OF THE MODEL

To replicate the transportation of entities along different pathways, we formulate a model that consists of two parallel one-dimensional lattices, identified as lane A and lane B, with each lane composed of L sites. The sites are enumerated as $i = 1, 2, \dots, L$, where the boundaries of each lane are represented by $i = 1$ and $i = L$, while the remaining sites constitute the bulk. In strict accordance with the hard-core exclusion principle, each lattice site is constrained to accommodate no more than a single particle. Particles experience horizontal drifting as they engage in unidirectional motion from the left to the right along the lanes. Moreover, these lanes allow vertical mobility of particles; specifically, lane A facilitates desorption, while lane B functions as an absorption pathway as shown in Fig. 1. The extreme boundaries of the lanes (at site $i = 1$ and $i = L$) are connected to a reservoir with a finite capacity. This naturally imposes a restriction on the overall number of particles in the system. Let us use the notation N_t to signify the total number of particles in the system and $N_r(t)$ to represent the number of particles in the reservoir at any instant of time. Note that the reservoir has abundant capacity to contain all the particles present in the system. Moreover, this restriction influences the rates at which particles flow from the reservoir into the lanes, which will be elucidated later. This arrangement creates a regulated environment in which the total number of particles on the lanes is determined by the interaction between the dynamics of interconnected lanes and the particle reservoir. At each time step, a site is chosen randomly and updated in accordance with the system's dynamic rules, which are delineated as follows:

(i) *Bulk sites*: For lane A, the displacement of a particle from the i th site relies on the status of the i th site on lane B. In case site i on lane B is vacant, a particle from the i th site of lane A is compelled to depart and then reconnects to the i th site on lane B at a unit rate. If the intended site on lane B is not vacant, then the particle is required to continue its horizontal movement along the lane with a unit rate, given that the neigh-

boring site is unoccupied. This indicates that a particle on lane A tends to prefer detachment over unidirectional movement.

(ii) *Entrance site*: A particle from the reservoir has the potential to enter through the first site $i = 1$ of lane A at a rate of $\bar{\alpha}$, given that the respective site is unoccupied. In the presence of a particle at this site, it initially attempts to attach to the first site of lane B. If this attachment is not achievable, then the particle then proceeds with its unidirectional movement along lane A.

(iii) *Exit site*: A particle positioned at the L th site on lane A first tries to detach from its lane and attach to the last site of lane B, given that the target site is unoccupied. If no successful attachment occurs, then the particle exits lane A at a rate of β to rejoin back the reservoir.

In lane B, particles enter from the initial site with a rate of $\bar{\alpha}$ and move along the lane from left to right at a unit rate, following the exclusion principle. On reaching the final site, they return to the reservoir with a rate of β . Additionally, each unoccupied site in lane B can absorb incoming particles from the corresponding vertical site in lane A at a unit rate.

The extreme ends of the lanes are connected to a limited particle reservoir, indicating that the total particle count remains conserved in the system. This conservation is expressed by the following equation:

$$N_t = N_r(t) + N_A(t) + N_B(t), \quad (1)$$

where $N_A(t)$ and $N_B(t)$ denote the number of particles on lanes A and B, respectively. Now implementing a global constraint on the total particle count results in the regulation of the inflow rate of particles into the lanes based on the number of particles present in the reservoir. Generally, a diminished particle count in the reservoir suggests lower entry rates, while an increased reservoir content corresponds to elevated entrance rates. Therefore, it is rational to consider the entrance rate [49] as follows:

$$\bar{\alpha} = \alpha \frac{N_r(t)}{N_t}. \quad (2)$$

Here α represents the inherent entrance rate of particles in the absence of any restrictions on the particle number. It is evident that $N_r(t) \leq N_t$ indicates that entry rates are bounded between 0 and α . As N_t tends towards infinity, the ratio N_r/N_t approaches 1, resulting in the convergence of $\bar{\alpha}$ to α . In this scenario, our model reduces to a well-examined two-lane coupled model with infinite resources [26,30]. If one eliminates the horizontal mobility of particles in lane B within the present model, then it transforms into the model discussed in Ref. [54] under specific conditions. Moreover, the current model can be conceptualized as two parallel exclusion lanes where lane A exhibits diffusive dynamics and serves as a feeder for lane B; meanwhile, lane B exclusively involves the one-dimensional transport of particles.

III. THEORETICAL APPROACH

The occupancy status of any site in the system can be expressed through a set of binary numbers denoted by τ_i and n_i for lanes A and B, respectively, where i signifies the site number. This variable τ_i (n_i) is assigned a “0” if the i th site on lane A (B) is unoccupied and a “1” if it contains a particle.

The temporal variations in particle occupancy in the bulk sites ($1 < i < L$) of both the lanes, as outlined by the master equations, can be stated as follows:

$$\langle \dot{\tau}_i \rangle = \mathcal{J}_{i-1}^A - \mathcal{J}_i^A - \mathcal{V}_i, \quad \langle \dot{n}_i \rangle = \mathcal{J}_{i-1}^B - \mathcal{J}_i^B + \mathcal{V}_i. \quad (3)$$

Here \mathcal{J}_i^j is the current passing from the site i to $i + 1$ in lane j , ($j \in \{A, B\}$) and \mathcal{V}_i is the vertical transverse current from lane A to B. Also, the symbol $\langle \dots \rangle$ represents the statistical average. The values of these particle currents involving one or two-point correlators can be expressed as

$$\mathcal{J}_i^A = \langle \tau_i(1 - \tau_{i+1})n_i \rangle, \quad \mathcal{J}_i^B = \langle n_i(1 - n_{i+1}) \rangle, \\ \mathcal{V}_i = \langle \omega \tau_i(1 - n_i) \rangle, \quad (4)$$

where $\omega = 1$ is the detachment or attachment rate from or to lane A or B. At the boundary sites ($i = 1, L$), we have

$$\langle \dot{\tau}_1 \rangle = \bar{\alpha} \langle (1 - \tau^1) \rangle - \mathcal{J}_1^A - \mathcal{V}_1, \\ \langle \dot{n}_1 \rangle = \bar{\alpha} \langle (1 - n^1) \rangle - \mathcal{J}_1^B + \mathcal{V}_1, \\ \langle \dot{\tau}_L \rangle = \mathcal{J}_{L-1}^A - \beta \langle \tau^L n^L \rangle - \mathcal{V}_L, \\ \langle \dot{n}_L \rangle = \mathcal{J}_{L-1}^B - \beta \langle n^L \rangle + \mathcal{V}_L. \quad (5)$$

To analyze this system further, it is often satisfactory to apply simple mean-field theory [55] in which the n -point correlation function is substituted with the product of n individual one-point correlator functions neglecting all possible correlations.

A. Continuum limit

We derive the continuum version of the proposed model by coarse-graining the discrete lattice with a lattice constant $\epsilon = 1/L$ and transforming both space and time as $x = i/L \in [0, 1]$ and $t' = t/L$, respectively. Replacing the discrete variables τ_i and n_i with continuous variables $\rho_i(x)$ and $\sigma_i(x)$, respectively, and retaining terms up to second order in the Taylor series expansion, we obtain

$$\frac{\partial \rho}{\partial t'} = \frac{\epsilon \sigma}{2} \frac{\partial^2 \rho}{\partial x^2} + \mathcal{J}^A \frac{\epsilon}{2} \frac{\partial^2 \sigma}{\partial x^2} + \epsilon(1 - \rho) \frac{\partial \rho}{\partial x} \frac{\partial \sigma}{\partial x} \\ - \sigma(1 - 2\rho) \frac{\partial \rho}{\partial x} - \mathcal{J}^A \frac{\partial \sigma}{\partial x} - L\rho(1 - \sigma), \quad (6)$$

$$\frac{\partial \sigma}{\partial t'} = \frac{\epsilon}{2} \frac{\partial^2 \sigma}{\partial x^2} - \frac{\partial \mathcal{J}^B}{\partial x} + L\rho(1 - \sigma). \quad (7)$$

Note that the subscript i is dropped as each lane is free from inhomogeneity of any kind. The symbols \mathcal{J}^A and \mathcal{J}^B describe the bulk mean-field particle currents in lanes A and B given by $\mathcal{J}^A = \rho(1 - \rho)$ and $\mathcal{J}^B = \sigma(1 - \sigma)$, respectively. The last term in both the Eqs. (6) and (7) is a result of vertical coupling between the lanes. It is important to note that this term involves multiplication by the lattice length L , indicating the need to rescale the coupling rates for observing competition between vertical and horizontal movements.

As the boundaries of each lane exhibit distinct behavior compared to the bulk, it is necessary to examine their evolution discretely, as outlined in Eq. (5). At the steady state and in the continuum limit ($L \rightarrow \infty$), the density evolution equations at the boundaries simplify to $\rho(0) = \sigma(0) = \bar{\alpha}$ and $\rho(1) = \sigma(1) = 1 - \beta$.

The quantity of our interest is the solution of the system at steady state which can be achieved by setting the time derivative equal to zero. Doing so leads to a set of singularly perturbed differential equations given by

$$\begin{aligned} \frac{\epsilon\sigma}{2} \frac{\partial^2 \rho}{\partial x^2} + \mathcal{J}^A \frac{\epsilon}{2} \frac{\partial^2 \sigma}{\partial x^2} + \epsilon(1-\rho) \frac{\partial \rho}{\partial x} \frac{\partial \sigma}{\partial x} \\ - \sigma(1-2\rho) \frac{\partial \rho}{\partial x} - \mathcal{J}^A \frac{\partial \sigma}{\partial x} - \rho(1-\sigma) = 0, \quad (8) \\ \frac{\epsilon}{2} \frac{\partial^2 \sigma}{\partial x^2} - \frac{\partial \mathcal{J}^B}{\partial x} + \rho(1-\sigma) = 0. \end{aligned}$$

Roughly speaking, in a singular perturbation problem [56], the transition as the limit $\epsilon \rightarrow 0$ is not gradual but rather abrupt. As the perturbation parameter ϵ diminishes, there is a sudden change in the nature of the problem. Typically, a singular perturbation problem arises when the perturbation parameter ϵ is introduced into a differential equation to scale the highest derivative in the equation. Consequently, as ϵ approaches 0, the order of the differential equation decreases, and the solution to the lower-order differential equation fails to satisfy all the boundary conditions or initial conditions at the same time. Thus, the solution experiences an abrupt cessation as ϵ tends to 0, indicating the formation of boundary layers. To find a global solution to the system, valid on the whole domain, we need to find two solutions: the inner solution and the outer solution. The outer solution captures the behavior away from the boundary layer, while the inner solution provides a detailed description of the boundary layer. Finally, it is essential to match these solutions effectively to derive the particle density at each site. We begin by exploring analytical and numerical methods to derive the outer solutions.

IV. BULK SOLUTION

Here we present two approaches for obtaining the outer solution or the bulk particle density for each lane.

A. Numerical technique

In this context, we outline an approach to deduce the density profile of the system by numerically solving the continuum formulations of the partial differential equations as presented in Eqs. (6) and (7). This technique offers two primary benefits. First, it is straightforward to implement and can be readily adapted for generalizations of the current model. Second, it proves valuable in situations where analytical treatment of the problem is unfeasible, providing an alternative means to derive solutions.

The initial step involves discretizing the partial differential equation using a finite-difference operator. In this process, the time derivative is substituted with a forward-difference formula, and the space derivative is replaced by a second-order central-difference operator. Set Δx as $1/L$, ($L < \infty$) and choose a suitable value for Δt to ensure that $|(\epsilon \Delta t)/(2(\Delta x)^2)| \leq 1$, which represents the stability criterion. Let $\rho_i^j(\sigma_i^j)$ represent the particle density of lane A (B) on site $i\Delta x$ and time step $j\Delta t$. Thus, we have the following

set of equations for the bulk sites $2 \leq i \leq L-1$:

$$\begin{aligned} \rho_i^{j+1} &= \rho_i^j + \frac{\epsilon \sigma_i^j \Delta t}{2\Delta x^2} (\rho_{i+1}^j - 2\rho_i^j + \rho_{i-1}^j) \\ &\quad + \rho_i^j (1 - \rho_i^j) \frac{\epsilon \Delta t}{2\Delta x^2} (\sigma_{i+1}^j - 2\sigma_i^j + \sigma_{i-1}^j) \\ &\quad + (1 - \rho_i^j) \frac{\epsilon \Delta t}{(2\Delta x)^2} (\rho_{i+1}^j - \rho_{i-1}^j) (\sigma_{i+1}^j - \sigma_{i-1}^j) \\ &\quad - \rho_i^j (1 - \rho_i^j) \frac{\Delta t}{2\Delta x} (\sigma_{i+1}^j - \sigma_i^j) \\ &\quad - \frac{\sigma_i^j \Delta t}{2\Delta x} (1 - 2\rho_i^j) (\rho_{i+1}^j - \rho_{i-1}^j) \\ &\quad - L\Delta t \rho_i^j (1 - \sigma_i^j), \\ \sigma_i^{j+1} &= \sigma_i^j + \frac{\epsilon \Delta t}{2\Delta x^2} (\sigma_{i+1}^j - 2\sigma_i^j + \sigma_{i-1}^j) \\ &\quad + (1 - 2\sigma_i^j) \frac{\Delta t}{2\Delta x} (\sigma_{i+1}^j - \sigma_{i-1}^j) \\ &\quad + L\Delta t \rho_i^j (1 - \sigma_i^j). \end{aligned} \quad (9)$$

Note that the above equations are not applicable for $i = 1$ and $i = L$. Therefore, we must formulate separate equations for these sites by employing Eq. (5), resulting in

$$\begin{aligned} \rho_1^{j+1} &= \rho_1^j + \frac{\alpha N_r \Delta t}{N_t} (1 - \rho_1^j) - \Delta t \rho_1^j \sigma_1^j (1 - \rho_2^j) \\ &\quad - L\Delta t \rho_1^j (1 - \sigma_1^j), \\ \sigma_1^{j+1} &= \sigma_1^j + \frac{\alpha N_r \Delta t}{N_t} (1 - \sigma_1^j) - \Delta t \sigma_1^j (1 - \sigma_2^j) \\ &\quad + L\Delta t \rho_1^j (1 - \sigma_1^j), \\ \rho_L^{j+1} &= \rho_L^j + \Delta t \sigma_{L-1}^j \rho_{L-1}^j (1 - \rho_L^j) - \Delta t \beta \rho_L^j \sigma_L^j \\ &\quad - L\Delta t \rho_L^j (1 - \sigma_L^j), \\ \sigma_L^{j+1} &= \sigma_L^j + \Delta t \sigma_{L-1}^j (1 - \sigma_L^j) - \Delta t \beta \sigma_L^j \\ &\quad + L\Delta t \rho_L^j (1 - \sigma_L^j), \end{aligned}$$

along with

$$N_r = N_t - \left(\sum_{i=1}^L \rho_i^j + \sum_{i=1}^L \sigma_i^j \right). \quad (10)$$

The solution is derived in the limit as j approaches infinity, ensuring that the system reaches its steady state. While this method easily produces the density profile, its effectiveness is limited when it comes to explicitly investigating additional stationary properties of the system. Moreover, this approach necessitates the independent study of each parameter, α , β , and μ , which is a cumbersome process for drawing concrete conclusions regarding the macroscopic behavior and stationary properties of the system.

In the following section, we derive explicit expressions for the particle densities and currents at each site within both lanes. These expressions will simplify our task and facilitate a more comprehensive analysis of the stationary properties.

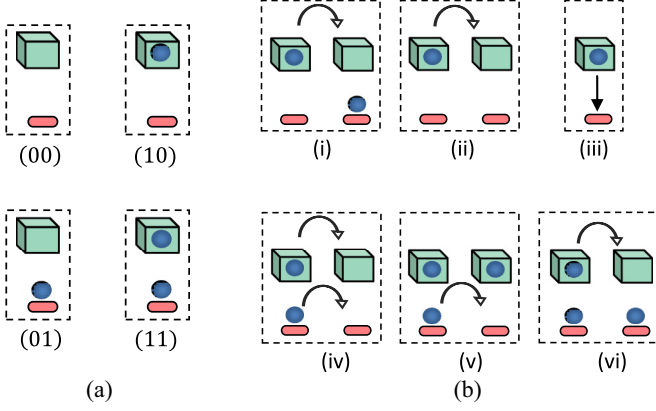


FIG. 2. (a) Possible states of a vertical cluster in the two-lane system. (b) Feasible transitions in a vertical cluster. (i) $P_{10}P_{01}$, (ii) $P_{10}P_{00}$, (iii) P_{10} , (iv) $P_{11}P_{00}$, (v) $P_{11}P_{10}$, and (vi) $P_{11}P_{01}$.

B. Cluster mean-field theory

To obtain explicit expressions for essential stationary properties in the current model, it is crucial to employ a theoretical framework that adequately accounts for correlations. An example of such a theory is the vertical cluster mean field, which specifically addresses the behavior of particles along the vertical direction. This methodology has proven to be valuable in accurately capturing the properties of various two-lane transport systems [26–30].

The current system allows for three types of vertical clusters: fully occupied, half-filled, and fully empty as shown in Fig. 2(a). In the case of a fully filled vertical cluster, denoted as (11), both sites are occupied. On the other hand, scenarios (01) and (10) represent half-filled situations, with particles located in either lane A or lane B, not both, respectively. Finally, an empty cluster is designated by (00). Let us define the probabilities for these potential configurations of a vertical cluster by P_{11} , P_{01} , P_{10} , and P_{00} . For the conservation of probabilities, it is necessary that

$$P_{00} + P_{10} + P_{01} + P_{11} = 1, \quad (11)$$

which is also called as the normalization condition. Thus, the bulk particle densities on each lane can be expressed by utilizing these vertical cluster probabilities as

$$\rho = P_{11} + P_{10}, \quad \sigma = P_{11} + P_{01}. \quad (12)$$

The absence of any form of inhomogeneity in the bulk indicates a reasonable assumption that the cluster probabilities remain unaffected by the spatial position of the vertical cluster. Thus, the master equation governing the evolution of these vertical clusters can be expressed as:

$$\begin{aligned} \frac{dP_{11}}{dt} &= P_{01}P_{10} + P_{11}P_{01} + P_{11}P_{10} - 2P_{11}P_{00} - P_{11}P_{01} \\ &\quad - P_{11}P_{10}, \end{aligned} \quad (13)$$

$$\frac{dP_{10}}{dt} = 2P_{11}P_{00} + P_{11}P_{10} - P_{10}. \quad (14)$$

Each expression on the right-hand side can be easily comprehended through the visual representations depicted in Fig. 2(b). The master equation corresponding to P_{01} can be formulated using a similar approach and deriving the

equation for P_{00} becomes straightforward by applying the normalization condition outlined in Eq. (11).

Our primary objective is to discern the solutions corresponding to the long-term behavior of the system. Consequently, we establish the following conditions:

$$\frac{dP_{00}}{dt} = \frac{dP_{10}}{dt} = \frac{dP_{01}}{dt} = \frac{dP_{11}}{dt} = 0. \quad (15)$$

By utilizing Eq. (11) as well as Eqs. (13) and (14) in Eq. (15), we derive the following set of equations:

$$2P_{11}P_{00} = P_{01}P_{10}, \quad 2P_{11}P_{00} + P_{11}P_{10} = P_{10}. \quad (16)$$

These equations can be solved concurrently, leading to two distinct scenarios:

$$(i) P_{10} = P_{11} = 0, \quad (ii) P_{10} = P_{00} = 0. \quad (17)$$

By applying the particle density expression for each lane as outlined in Eq. (12) to the above equations, we can draw two conclusions: In scenario (i) lane A displays zero particle density, whereas in (ii) lane B is entirely occupied with a particle density of 1.

Before proceeding with further analysis, it is essential to highlight that the system is subject to open boundary conditions. To conduct a comprehensive examination of the system, one must account for both the entry and exit currents from the system, represented by the following equations:

$$\begin{aligned} \mathcal{J}^A(0) &= \bar{\alpha}(1 - P_{11} - P_{10}), \\ \mathcal{J}^B(0) &= \bar{\alpha}(1 - P_{11} - P_{01}), \\ \mathcal{J}^A(1) &= \beta P_{11}, \\ \mathcal{J}^B(1) &= \beta(P_{11} + P_{01}). \end{aligned} \quad (18)$$

Similarly, the bulk current for each lane can be stated by

$$\begin{aligned} \mathcal{J}^A &= P_{11}(1 - P_{11} - P_{10}), \\ \mathcal{J}^B &= P_{11} + P_{01}(1 - P_{11} - P_{01}). \end{aligned} \quad (19)$$

As the particle current remains consistently continuous across the system, it allows us to establish a relationship between the bulk and boundary currents:

$$\mathcal{J}^A(0) + \mathcal{J}^B(0) = \mathcal{J}^A + \mathcal{J}^B = \mathcal{J}^A(1) + \mathcal{J}^B(1). \quad (20)$$

Now, we can leverage the fact that the system is connected to a finite particle reservoir with a reservoir occupancy of N_r . Returning to the particle number conservation (PNC) equation, as expressed in Eq. (1), we can restate it as:

$$\frac{N_t}{2L} = \frac{N_r}{2L} + \frac{1}{2} \left(\frac{N_A}{L} + \frac{N_B}{L} \right), \quad (21)$$

or, in a more simplified form:

$$\mu = \rho_r + \frac{1}{2} \left[\int_0^1 \rho(x) dx + \int_0^1 \sigma(x) dx \right]. \quad (22)$$

In this context, $\mu = N_t/(2L)$ signifies the filling factor, which is a measure of the ratio of the total number of particles to the total number of sites in a system. Furthermore, we employ the variable ρ_r to denote the reservoir density.

Now, with all the essential components in hand, our attention shifts to a comprehensive analysis of the important stationary properties of the system. The objective is to derive explicit expressions for both particle densities and reservoir

density. This will be achieved by leveraging the solutions obtained from the vertical master equation, as indicated by Eq. (17), and by incorporating the principles of current continuity, as expressed in Eq. (21), and particle number conservation, as given in Eq. (23). These explicit expressions will subsequently be employed to quantify the stationary characteristics of the system, encompassing phase diagrams, density profiles, particle currents, and potential phase transitions.

To investigate the influence of finite resources on a two-lane system, we examine the dynamic characteristics across the parameter space defined by α and β . Our examination encompasses a thorough inspection of various stationary system properties, including density profiles, particle currents, and probable phase transitions. In the context of a one-dimensional open TASEP with infinite particle resources and boundary parameters, α and β , previous studies have identified three stationary phases [13,14,16]: LD, HD, and MC phases. Notably, a delocalized shock phase is confined to a specific line in the phase plane. However, when the particle species are constrained in number, the originally delocalized shock phase undergoes a transformation. It evolves into a localized shock phase that manifests across a substantial region of the phase plane, resulting in an increase in the number of phases to four [49].

Now let us explore the possible stationary phases that could endure in the two-lane strongly coupled system with constrained resources. To begin, we employ the notation P/Q to represent a phase of the system, where P and Q signify a phase manifested by lanes A and B, respectively. Derived from the two solutions to vertical probabilities outlined in Eq. (17), two distinct scenarios emerge. In case (i), lane A exhibits zero particle density, whereas in case (ii), lane B is completely filled with a maximum particle density of 1. Both of these cases depict a condition of zero particle current, leading us to label the corresponding phases in the respective lanes as ZC_0 and ZC_1 , where the subscript indicates the particle density. In each of these situations, the opposing lane can manifest any of the four phases: LD, HD, MC, and S. Now we examine each of these situations individually.

1. Zero particle current in lane A: (ZC_0/Q)

Let us start by considering the scenario where $P_{10} = P_{11} = 0$. According to Eq. (12), we get $\rho = 0$, signifying the case of zero particle density in lane A. Consequently, the particle currents given by Eqs. (19) and (20) are simplified to

$$\begin{aligned}\mathcal{J}^A(0) &= \bar{\alpha}, \quad \mathcal{J}^B(0) = \bar{\alpha}(1 - P_{01}), \\ \mathcal{J}^A &= 0, \quad \mathcal{J}^B = P_{01}(1 - P_{01}), \\ \mathcal{J}^A(1) &= 0, \quad \mathcal{J}^B(1) = \beta P_{01}.\end{aligned}\quad (23)$$

With $P_{10} = 0$ and $P_{11} = 0$ in this system, the vertical cluster (01) can be interpreted as particles, and the corresponding holes are denoted by (00). Thus, the two-lane system can be viewed as one-lane system with some entrance rate α_{eff} and exit rate β . Here lane A is in the ZC_0 phase and the other lane can assume one of the following phases: LD, HD, MC, or S. Now we scrutinize each of these phases individually.

(i) ZC_0/LD phase. In this entrance-dominated phase, the particle current is governed by the entry parameter implying

that $P_{01} = \alpha_{\text{eff}}$. By utilizing the continuity of current across the lanes, we can write

$$\alpha_{\text{eff}}(1 - P_{01}) = \mathcal{J}^A(0) + \mathcal{J}^B(0) = \mathcal{J}^A + \mathcal{J}^B,$$

which is equivalent to

$$\alpha_{\text{eff}}(1 - P_{01}) = \bar{\alpha} + \bar{\alpha}(1 - P_{01}).$$

The above can be solved to calculate the expression for the effective entrance rate as

$$\alpha_{\text{eff}} = \frac{1}{2}[1 + \bar{\alpha} - \sqrt{(1 + \bar{\alpha})^2 - 8\bar{\alpha}}], \quad (24)$$

which is valid for $\bar{\alpha} < \frac{1}{6}$. We must recall that the parameter $\bar{\alpha}$ is regulated by the reservoir density ρ_r and the filling factor μ . Thus, we exploit the particle conservation criteria given by Eq. (22), which can be restated as

$$\mu = \rho_r + \frac{\alpha_{\text{eff}}}{2} \quad (25)$$

and solved to determine the value of reservoir density as

$$\begin{aligned}\rho_r &= \frac{1}{2(\alpha + 2\mu)}[\alpha(\mu - 1) + \mu(4\mu - 1) \\ &\quad + \sqrt{\alpha^2(\mu - 1)^2 + 2\alpha(1 - 3\mu)\mu + \mu^2}].\end{aligned}\quad (26)$$

The existential criteria for this phase can be written as follows:

$$\alpha_{\text{eff}} < \beta, \quad \bar{\alpha} < \frac{1}{6}. \quad (27)$$

In the limit, $\mu \rightarrow \infty$, $\bar{\alpha}$ tends to converge to α . This results in the effective rate α_{eff} matching the calculated effective rate for this phase when resources are infinite, as detailed in Ref. [26].

(ii) ZC_0/HD phase. Here lane A remains in the zero current phase while lane B displays the high-density phase. The current continuity equation in this case takes a simplified form

$$P_{01}(1 - P_{01}) = \beta P_{01} \Rightarrow P_{01} = 1 - \beta. \quad (28)$$

Utilizing PNC, we retrieve the reservoir density $\rho_r = \frac{2\mu-1+\beta}{2}$. The feasible region corresponding to phase requires β to remain less than 0.5 and the effective entrance rate which leads to

$$\frac{2\mu\beta(1 - \beta)}{(2 - \beta)(2\mu - 1 + \beta)} < \alpha < \frac{2\beta\mu}{(2\mu - 1 + \beta)}. \quad (29)$$

Clearly, when $\mu \rightarrow \infty$, the condition for the existence of a (0/HD) phase in a system with no constraint on particle resources is recovered [26].

(iii) ZC_0/MC phase. Let us assume that lane B exhibits maximal current phase with particle density given by 0.5 and current equal to 0.25. In such a scenario, we get $P_{00} = P_{01} = 0.5$. By particle number conservation, the value of reservoir density can be procured as

$$\rho_r = \mu - \frac{1}{4}. \quad (30)$$

Moreover, the other parameters are $\alpha_{\text{eff}} = 3\bar{\alpha}$ and $\bar{\alpha} = \frac{\alpha(4\mu-1)}{4\mu}$. Using all these expressions, the condition for the existence of this phase can be framed by

$$\max\{\bar{\alpha}, \frac{1}{2}\} < \beta, \quad \frac{1}{6} < \bar{\alpha} < \frac{1}{2}. \quad (31)$$

As μ approaches infinity, the expression for the effective entry rate coincides with the scenario involving infinite resources, as documented in Ref. [26].

(iv) ZC_0/S phase. Presume that lane A displays particle density 0, while lane B exhibit a discontinuity in the density profile connecting a section of low density on the left to a

section of high density on the right. We prefer to denote the position of this sudden transition in lane B by x_B .

As lane B is in the low-density phase on the left, we observe that $P_{01} = \alpha_{\text{eff}}$ near the left boundary, and the effective entrance rate remains the same, as indicated by Eq. (24). The criteria for the persistence of the shock phase require that the entry rate must be equal to the exit rate, thus leading to

$$\rho_r = \frac{\beta\mu(1-\beta)}{\alpha(2-\beta)}. \quad (32)$$

The only variable remaining to be determined is the position of the shock, which can be derived from the conservation of particles and expressed in a simplified form as follows:

$$x_B = \frac{1-\beta-2(\mu-r)}{\alpha(2-\beta)}. \quad (33)$$

Finally, the boundary parameters must satisfy the following to display this phase:

$$0 < x_B < 1, \quad \beta < 0.5. \quad (34)$$

This phase ceases to exist in case $\mu \rightarrow \infty$.

2. Zero particle current in lane B: (P/ZC₁)

Now, let us consider the alternate scenario where $P_{00} = P_{10} = 0$. As a consequence, the particle density in lane B reaches its maximum value of 1, resulting in zero particle current. The revised value of the particle currents are detailed as follows:

$$\begin{aligned} \mathcal{J}^A(0) &= \bar{\alpha}(1 - P_{11}), \quad \mathcal{J}^B(0) = 0, \\ \mathcal{J}^A &= P_{11}(1 - P_{11}), \quad \mathcal{J}^B = 0, \\ \mathcal{J}^A(1) &= \beta P_{11}, \quad \mathcal{J}^B(1) = \beta. \end{aligned} \quad (35)$$

In this situation, particles in lane B are represented by the fully filled vertical cluster (11), while a vacancy corresponds to (10). Consequently, in this case, the two-lane system can be conceptualized as a one-dimensional TASEP system with an entry rate of $\bar{\alpha}$ and an effective exit rate denoted by β_{eff} . Also, lane B remains in the ZC₁ phase, while lane A can exhibit any of the four phases: LD, HD, MC, and S.

(i) HD/ZC₁ phase. The stationary particle density of lane A is given by $1 - \beta_{\text{eff}}$, while that of lane B is 0. This relationship implies that $P_{11} = 1 - \beta_{\text{eff}}$. Applying the current continuity principle, we can express it as:

$$P_{11}(1 - P_{11}) = \beta P_{11} + \beta = \beta_{\text{eff}} P_{11}. \quad (36)$$

Solving this equation yields the value of the effective exit rate:

$$\beta_{\text{eff}} = \frac{1}{2}[1 + \beta - \sqrt{(1 + \beta)^2 - 8\beta}]. \quad (37)$$

Now we make use of Eq. (22) to calculate reservoir density as

$$\rho_r = \frac{1}{4}(\beta - 3 + 4\mu - \sqrt{1 - 6\beta + \beta^2}). \quad (38)$$

Finally, the conditions fulfilled by this phase are delineated as:

$$\beta_{\text{eff}} < \bar{\alpha}, \quad \beta < \frac{1}{6}. \quad (39)$$

(ii) LD/ZC₁ phase. During this phase, we assume that lane A portray the LD phase. In such scenarios, $P_{11} = \bar{\alpha}$ and the reservoir density is given by

$$\rho_r = \frac{\mu(2\mu - 1)}{\alpha + 2\mu}. \quad (40)$$

Under these circumstances, the existential condition for this phase is

$$\frac{\bar{\alpha}(1 - \bar{\alpha})}{2 - \bar{\alpha}} < \beta < \bar{\alpha} < \frac{1}{2}. \quad (41)$$

(iii) MC/ZC₁ phase. During this phase, lane A experiences a maximal current phase with particle density given by 0.5. So we have $P_{11} = P_{01} = 0.5$. The resulting reservoir density is given by:

$$\rho_r = \mu - \frac{3}{4}. \quad (42)$$

The effective exit rate can be obtained in a straightforward manner as $\beta_{\text{eff}} = 1 - \beta$. Therefore, this phase persists only when:

$$\frac{1}{6} < \beta < \frac{1}{2} < \bar{\alpha}. \quad (43)$$

(iv) S/ZC₁ phase. In this scenario, a shock persists in lane A, linking a segment with particle density $\bar{\alpha}$ on the left to a region with particle density $1 - \beta_{\text{eff}}$ on the right, separated at the point denoted by x_A . The effective exit rate retains the same value as expressed in Eq. (37). For lane A to display the shock phase, it must adhere to the condition $\bar{\alpha} = \beta_{\text{eff}}$, providing us with the reservoir density expressed as:

$$\rho_r = \frac{\mu(1 + \beta - \sqrt{1 - 6\beta + \beta^2})}{2\alpha}. \quad (44)$$

Revisiting Eq. (22) allows us to calculate the shock position in this case, given by:

$$x_A = \frac{2 - \bar{\alpha} - 2(\mu - r)}{1 - 2\bar{\alpha}}. \quad (45)$$

Hence, the determined region for this phase must meet the criteria of $0 < x_A < 1$ in conjunction with $\bar{\alpha} < 0.5$. This phase vanishes when μ tends to 0.

In addition to the aforementioned phases, several other phases are observed, arising from the combination of the two scenarios. During these phases, certain region of the system exhibit P/ZC₁, while the remaining part displays ZC₀/Q. Considering that particle current must remain continuous across each lane, these two scenarios can be appropriately aligned.

3. Other phases

We choose to represent these phases as R-S/M-N, where R (S) indicates the type of stationary phase on the left (right) of lane A, while M (N) denotes the stationary phase on the left (right) of lane B. The stationary properties for such phases are as follows:

(i) LD-ZC₀/ZC₁-HD phase. In this phase, we observe a LD/ZC₁ phase on the left connected to a ZC₀/HD region on the right, and the position of the domain wall in the lanes is represented by x_A and x_B . As mentioned previously, this phase can be visualized as two single-lane TASEP models. One has an entry rate of $\bar{\alpha}$ and an exit rate of β_{eff} , while the other has $\alpha_{\text{eff}} - \beta$ as the boundary parameters.

To ensure current continuity in the system, the shock position must be synchronized between both lanes. Therefore, we employ the notation x_s to represent the common shock position. Additionally, for the system to maintain the shock phase, we must have $\alpha_{\text{eff}} = \beta_{\text{eff}}$, which leads to the condition $\bar{\alpha} = \beta$, enabling us to derive the reservoir density as $\rho_r = \frac{\beta\mu}{\alpha}$.

To determine the position of the shock in this phase, we use the conservation of particles, transforming Eq. (22) into:

$$\mu = \rho_r + \frac{1}{2} \left[\int_0^{x_s} (\bar{\alpha} + 1) dx + \int_{x_s}^1 (0 + 1 - \beta) dx \right], \quad (46)$$

which yields

$$x_s = \frac{2(\mu - r) - (1 - \beta)}{2\beta}. \quad (47)$$

Thus, the identified region in the phase diagram corresponding to this phase is

$$0 < x_s < 1, \quad \beta < 0.5. \quad (48)$$

In the presence of an infinite supply of particles, this phase does not persist.

(ii) MC-ZC₀/ZC₁-MC phase. Here the left bulk of the system remains in the MC/ZC₁ phase while the right bulk displays the ZC₀/MC phase. As elaborated on in the preceding case, the synchronization of the shock position between two lanes is evident. Specifically, the particle density in each lane can be written as

$$\rho = \begin{cases} 0.5, & \text{if } 0 < x < x_s \\ 0, & \text{if } x_s < x < 1, \end{cases} \quad (49)$$

$$\sigma = \begin{cases} 1, & \text{if } 0 < x < x_s \\ 0.5, & \text{if } x_s < x < 1, \end{cases}$$

where x_s gives the common shock position. Therefore, this phase is entirely dominated by the bulk. The position of the shock can be determined by applying particle-hole symmetry.

In the limit as μ approaches infinity, the shock position stabilizes at 0.5 [26], leading us to characterize this phase as a Meissner phase.

The analysis presented thus far yields the outer solution, representing the bulk particle density for both lanes. Now we will explore the methodology for calculating the inner solutions associated with each phase.

V. INNER SOLUTION: BOUNDARY-LAYER ANALYSIS

To elucidate the characteristics of the boundary layer, we first analyze the behavior of the system in the thermodynamic limit. Under this condition, Eq. (8) transforms into a set of first-order differential equations, each accompanied by two boundary conditions, resulting in an overdetermined system. In such cases, a boundary layer is observed either within the bulk or at the boundaries. The solution of the first-order differential equations is called the outer or bulk solution and delineates the major portion of the density profile, whose thorough analysis has been conducted in the preceding section. Such a solution will be denoted by ρ_b and σ_b for the two lanes.

Here we provide a summary of the methodology associated with obtaining the boundary-layer solution. For a comprehensive understanding, readers can refer to Ref. [57]. The outer solution satisfies a first-order differential equation, accommodating at most a single boundary condition. To address the other condition, a boundary layer emerges within the density profile. This layer must adhere to two essential criteria: (i) It must fulfill the other boundary condition and (ii) it must asymptotically approach the outer solution. Generally, the boundary layer satisfies one boundary condition, while the

outer solution addresses the other. Nevertheless, in certain scenarios, a boundary layer within the system's bulk can separate two outer solutions, each of them meeting one of the boundary conditions. Therefore, it can be concluded that the presence of this layer is not confined solely to the peripheries or boundaries of the system. This boundary-layer solution is referred to as the inner solution and is denoted by ρ_{in}/σ_{in} .

In the preceding section, we have successfully determined the outer solution by examining two distinct situations: the first involving zero particle current along with density zero in lane A and the second featuring zero particle current in lane B but with a maximum particle density set at 1. Since the boundary-layer solution must asymptotically align with the outer solution, it is crucial to compute the inner solution while taking into account the characteristics of the outer solution.

A. Zero particle current in lane A

As elucidated earlier, the stationary characteristics in this scenario are dictated by Eq. (23), where both the particle current and density in the bulk as well as at the exit sites of lane A are precisely zero, but a nonzero particle current is present at the entrance site. Consequently, we expect the existence of a boundary layer merely at the left boundary in lane A.

Our primary objective now is to compute the boundary layer or the inner solution pertaining to lane B. We have the following continuum system at the steady state:

$$\frac{\epsilon}{2} \frac{\partial^2 \sigma}{\partial x^2} + (1 - 2\sigma) \frac{\partial \sigma}{\partial x} = 0. \quad (50)$$

To derive a boundary-layer solution, it is convenient to introduce a rescaled variable, denoted as $a = (x - x_0)/\epsilon$, where x_0 signifies the location of the boundary layer. If there is a boundary layer at the left end, then x_0 is set at 0, and with ϵ approaching 0 ($L \rightarrow \infty$), the variable a tends towards ∞ . Similarly, in case $x_0 = 1$, then $a \rightarrow -\infty$ as $\epsilon \rightarrow 0$.

Now, in terms of the rescaled position, the differential equation given by Eq. (50) gets modified to

$$\frac{1}{2} \frac{d^2 \sigma_{in}}{da^2} + (2\sigma_{in} - 1) \frac{d\sigma_{in}}{da} = 0, \quad (51)$$

which on integrating once yields

$$\frac{1}{2} \frac{d\sigma_{in}}{da} - \sigma_{in}(1 - \sigma_{in}) = k_0, \quad (52)$$

where k_0 is the constant of integration. Calculating the value of this constant using the criteria that the inner solution must saturate to the outer solution gives $k_0 = \sigma_b(\sigma_b - 1)$. Further integration yields the following:

$$\sigma_{in}(a) = \frac{1}{2} + \frac{|2\sigma_b - 1|}{2} \coth(a|2\sigma_b - 1| + k_2),$$

$$\sigma_{in}(a) = \frac{1}{2} + \frac{|2\sigma_b - 1|}{2} \tanh(a|2\sigma_b - 1| + k_2). \quad (53)$$

Here $\frac{1}{|2\sigma_b - 1|}$ is the width of the boundary layer with respect to a and the constant k_2 gives the center of the boundary layer. Moreover, these constants depend on the boundary condition that the inner solution satisfy.

We adopt the notation T_k/C_k to describe a boundary layer of tanh / coth type as given by Eq. (53) for the different phases of the system. Here k can take the values l , b , or r , indicating the presence of a boundary layer at the left end, in the bulk, or at the right end, respectively.

In the following discussion, we scrutinize each of the previously mentioned scenarios regarding the outer solution for their corresponding boundary-layer solutions.

(i) ZC_0/LD phase. In this particular case, the outer solution for lane B satisfies the left boundary condition at $x = 0$, clearly indicating the manifestation of a boundary layer at the right end. Here the corresponding bulk densities are $\rho_b = 0$ and $\sigma_b = \alpha_{\text{eff}}$, where α_{eff} is determined by Eq. (24).

In lane A, only the entry current is nonzero, giving rise to a boundary layer of C_l type characterized by a positive slope. On the other lane, two distinct types of boundary-layer solutions appear in the vicinity of the boundary at $x = 1$ depending on the entry-exit parameters. When $\alpha_{\text{eff}} < 1 - \beta$, the boundary layer exhibits a positive slope, and the corresponding inner solution follows a tanh-type profile. Conversely, when $\alpha_{\text{eff}} > 1 - \beta$, the boundary layer displays a negative slope, and the inner solution takes on a coth-type profile. Thus the two types of boundary layers in this case are denoted by C_l/T_r and C_l/C_r which are separated by the boundary $\alpha_{\text{eff}} = 1 - \beta$. We prefer to use the term “surface transitions” to describe such changes occurring within a specific phase.

(ii) ZC_0/HD phase. Similarly to the previous case, a boundary layer of C_l type emerges in lane A. The outer solution in lane B is an exit-dominated phase and adheres to the right boundary condition, while the inner solution satisfies the condition at $x = 0$. When $1 - \beta < \alpha_{\text{eff}}$, the boundary layer must have a positive slope, making it necessary to employ a coth-type inner solution. Conversely, when $1 - \beta > \alpha_{\text{eff}}$, the boundary layer, featuring a negative slope, is associated with a tanh-type solution. Therefore, the boundary-layer solution C_l/T_l is distinguished from C_l/C_l by the line $\alpha_{\text{eff}} = 1 - \beta$.

(iii) ZC_0/S phase. In this context, a stationary shock emerges in the density profile of lane B, connecting a region of LD phase with a particle density of $\alpha_{\text{eff}} = \bar{\alpha}$ to an HD phase with density, $1 - \beta$. The position of this shock is denoted as x_B and is determined by Eq. (33). Consequently, the outer solution comprises of two segments: one with a density less than 0.5 (on the left) and the other greater than 0.5. This gives rise to a boundary layer of the tanh-type, thus labeled as C_l/T_b .

(iv) ZC_0/MC phase. Here lane B exhibits a maximal current phase where the bulk density is precisely equals 0.5. To satisfy the two boundary conditions, specifically $\sigma(0) = \bar{\alpha}$ and $\sigma(1) = 1 - \beta$, a boundary layer must be present at each end. The conditions for the existence of this phase are $\bar{\alpha} > 0.5$ and $\beta > 0.5$, implying that $\sigma(1) < 0.5 < \sigma(0)$. Consequently, a boundary layer of coth type appears at both ends and can be denoted as $C_l/C_{l,r}$.

B. Zero particle current in lane B

The stationary particle currents in this instance are determined by Eq. (36), indicating the emergence of a boundary layer on the right boundary of lane B. Following a similar pro-

cedure as in the previous case, two types of boundary layers are identified, labeled as tanh-type and coth-type. Hence, the respective inner solutions demonstrated in the phases of this category can be expressed as follows:

(i) HD/ZC_1 phase. In this case, two distinct types of boundary conditions are observed: T_l/C_r and C_l/C_r , which are distinguished by the line $\bar{\alpha} = 1 - \beta_{\text{eff}}$.

(ii) LD/ZC_1 phase. A tanh-type boundary layer is observed in lane A when $\bar{\alpha} < 1 - \beta_{\text{eff}}$, whereas it is of coth-type when $\bar{\alpha} > 1 - \beta_{\text{eff}}$.

(iii) S/ZC_1 phase. A stationary shock phase manifests in the density profile with the shock position denoted as x_A . The corresponding boundary layer is characterized by T_b/C_r .

(iv) MC/ZC_1 phase. In this case, a boundary layer of the type $C_{l,r}/C_r$ emerges in the density profile.

C. Combination of P/ZC_1 and ZC_0/Q phases

As previously explained, in such phases, lane A exhibits the $P-ZC_0$ phase, while the other displays the ZC_1-Q phase.

(i) $LD-ZC_0/ZC_1$ -HD phase. The solution for the bulk of the density profile is

$$\rho = \begin{cases} \bar{\alpha}, & \text{if } 0 < x < x_s \\ 0, & \text{if } x_s < x < 1, \end{cases}$$

$$\sigma = \begin{cases} 1, & \text{if } 0 < x < x_s \\ 1 - \beta, & \text{if } x_s < x < 1. \end{cases} \quad (54)$$

In this phase, the boundary layer is not limited to the boundaries; rather, it manifests in the bulk in the form of a shock at the position x_s , thus taking on the form of C_b/C_b .

(ii) $MC-ZC_0/ZC_1$ -MC phase. Applying a similar approach, in this case, a boundary layer of the type $C_{l,b}/C_{b,r}$ emerges.

VI. RESULTS AND DISCUSSION

In this section, we conduct a thorough exploration of the steady-state characteristics within the proposed model, with a particular emphasis on the stationary phase diagrams. We utilize theoretical expressions for the outer solution and findings from boundary-layer analysis to scrutinize the system's behavior in the $\alpha - \beta$ space. To validate the theoretical findings, we perform kinetic Monte Carlo simulations (akin to the Gillespie algorithm) with the lattice size of each lane $L = 1000$. For a given system state, the algorithm identifies all potential sites for a successful move, computes their kinetic rates, and sums them. The event probability is then determined by weighing each rate against the total rate. The time until the next event is calculated as $\Delta t = -\ln(r)/(\text{sum of all kinetic rates})$, where r is a random number generated from a uniform distribution between 0 and 1. The lists are updated accordingly, and the process is iterated until 10^9 number of events have occurred. To ensure the system reaches a steady state, the initial 5% of these events are excluded. These simulation points are graphed with an accuracy of less than 2% in each figure, a precision reflected by the size of the symbols employed in the plots.

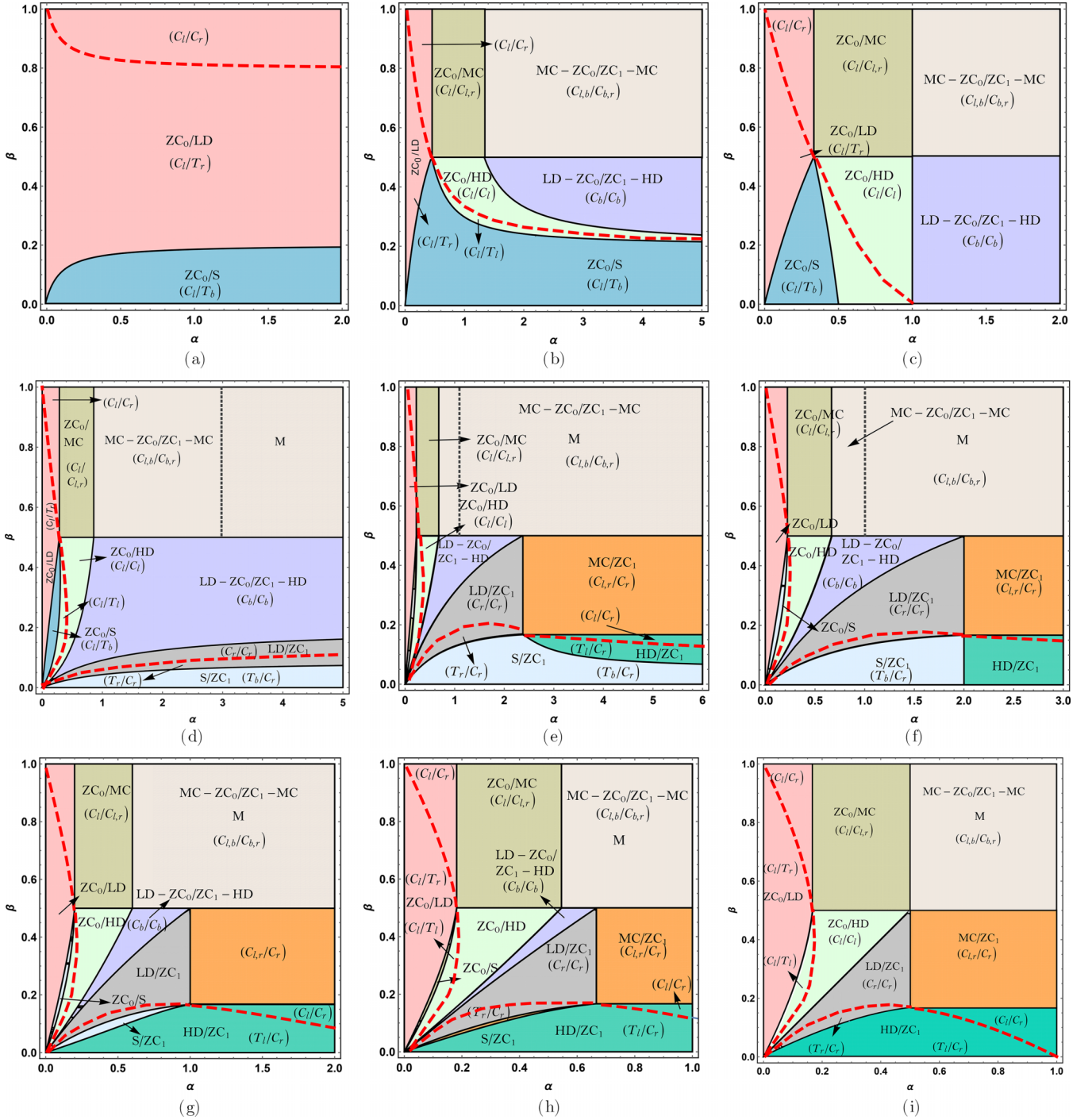


FIG. 3. Phase diagrams for stationary states for different values of μ : (a) $\mu = 0.1$, (b) $\mu = 0.4$, (c) $\mu = 0.5$, (d) $\mu = 0.6$, (e) $\mu = 0.9$, (f) $\mu = 1$, (g) $\mu = 1.5$, (h) $\mu = 3$, and (i) $\mu \rightarrow \infty$. Each diagram delineates both bulk and surface transitions, categorized through boundary-layer analysis. Solid lines denote bulk transitions, while dashed (thick red) lines describe surface transitions. M designates the Meissner phase corresponding to $MC-ZC_0/ZC_1-MC$ phase which is independent of the boundary parameters.

A. Stationary phase diagrams

We examine the stationary behavior of the system under different filling factors in the $\alpha - \beta$ phase plane. The values of μ are selected such that they explain all the possible and crucial structural changes in the phase diagrams.

Figure 3 presents stationary phase diagrams for various filling factor values, capturing topological changes and pro-

viding a comprehensive characterization of phases through their boundary layers. Solid lines denote bulk transitions, while dashed lines indicate surface transitions. The notation (M_k, N_k) represents the boundary layer, where $M, N \in \{T, C\}$ signifies the type of the tanh-type/coth-type boundary layer and $k \in \{l, b, r\}$ describes its position, the left boundary, bulk, or the right boundary. Theoretical critical values for μ that correspond to qualitative changes can be obtained from

Eqs. (30), (41), and (39) and are given by

$$\mu_{c_1} = 0.25, \quad \mu_{c_2} = 0.5, \quad \text{and} \quad \mu_{c_3} = 0.75. \quad (55)$$

For $\mu \leq \mu_{c_1}$, the phase diagram is characterized by only two stationary phases: ZC_0/LD and ZC_0/S [refer to Fig. 3(a)]. As μ increases within the range $\mu_{c_1} \leq \mu \leq \mu_{c_2}$, four distinct phases emerge, namely ZC_0/HD , ZC_0/MC , $LD-ZC_0/ZC_1-HD$, and $MC-ZC_0/ZC_1-MC$, as evident from Fig. 3(b). Beyond the critical value μ_{c_2} , the system undergoes substantial topological changes both qualitatively and quantitatively, with the addition of LD/ZC_1 and S/ZC_1 phases. So the phase schema now exhibits a total of eight phases, as depicted in Fig. 3(d). The domain occupied by the $MC-ZC_0/ZC_1-MC$ phase can be classified into two types. In one, the position of the shock is contingent on the boundary parameters $\alpha - \beta$, while in the other, the position is consistently fixed at 0.5, no longer influenced by the rates α and β . Thus, the latter case can be categorized as a Meissner phase. After the critical value μ_{c_3} , two new phases emerge in the phase diagram namely, MC/ZC_1 and HD/ZC_1 , as shown in Fig. 3(e). At this point, the phase diagram displays the maximum number of phases and includes all possible phases for the system. A further increase in the value of μ results in the shrinkage and expansion of the phase regions [see Fig. 3(f)–3(h)]. Finally, in the limit $\mu \rightarrow \infty$, the phase diagram becomes much simpler, consisting of only seven phases as shown in Fig. 3(i) and the results of Ref. [26] are recovered.

Now we emphasize a few observations that can be derived from these phase diagrams. In all the phases of the form ZC_0/Q where $Q \in \{LD, HD, MC, S\}$, as confirmed by Eq. (23), particles enter both lanes but exit exclusively from lane B. The detachment (attachment) of particles from (to) lane A (B) compels the particles to swiftly shift to lane B on entry through lane A. Consequently, particle progression occurs solely along lane B. In phases exhibiting zero particle current in lane B and density equal to 1 (P/ZC_1 form), particles enter exclusively through lane A, yet they exit through both lanes. It is evident from Fig. 3 that these phases exist primarily for smaller values of β , indicating that a slow exit rate results in the accumulation of particles in lane B until a point is reached where no particle movement becomes possible. Thus, the mobility of the particles is only possible in lane A.

A noteworthy observation in the current system is the identification of two phases characterized by downward shocks. Typically a downward shock refers to a sudden and significant decrease in the particle density. Such types of shocks are observed in the $LD-ZC_0/ZC_1-HD$ phase and $MC-ZC_0/ZC_1-MC$ phase. In the $LD-ZC_0/ZC_1-HD$ phase, the position of the downward shock is given by Eq. (47) which depends on two parameters, μ and β . This shock links a segment in the low-density phase on the left to the zero-density phase on the right in lane A. Simultaneously, in lane B, it connects a region with particle density 1 on the left to the high-density phase on the right. Furthermore, the location of this downward shock is coordinated in both lanes. A similar observation applies to the $MC-ZC_0/ZC_1-MC$ phase, but the downward shock remains within the interval $[0, 0.5]$. When this position is precisely equal to 0.5, we prefer to characterize the phase as the Meissner phase, as in this case, the density profiles are independent of the boundary parameters $\alpha - \beta$. In these phases, the entry

of the particles is limited solely through lane A. However, owing to the attachment-detachment mechanism, their exit is exclusively facilitated through lane B. Now we will discuss each of these shock phases in detail in the upcoming section.

B. Shock dynamics and phase transitions

In this section, we commence our discussion by scrutinizing the characteristics of the diverse types of shocks present in the system. There are four phases involving a discontinuity in the density profiles, namely ZC_0/S , S/ZC_1 , $LD-ZC_0/ZC_1-HD$, and $MC-ZC_0/ZC_1-MC$. In the former two phases, there is an upward shock confined to only one lane. Conversely, the latter two phases display a synchronized downward shock in both lanes.

1. Upward unsynchronized shock

Initially, our attention is directed towards examining how the shock propagates in the ZC_0/S and S/ZC_1 phases concerning variations in both the entry and exit rates. This analysis relies on the analytical expression derived in Sec. IV B 1 and IV B 2. The shock's velocity in ZC_0/S and S/ZC_1 phases is given by

$$V = \begin{cases} \beta - \alpha_{\text{eff}}, & \text{for } ZC_0/S \text{ phase,} \\ \beta_{\text{eff}} - \bar{\alpha}, & \text{for } S/ZC_1 \text{ phase,} \end{cases}$$

where α_{eff} and β_{eff} is given by Eq. (25) and (38), respectively. To achieve a stationary shock, the velocity must be zero, indicating that $\beta = \alpha_{\text{eff}}$ and $\beta_{\text{eff}} = \bar{\alpha}$. The position of the shock can be represented as follows:

$$x_B = \frac{1 - \beta - 2(\mu - r)}{\alpha(2 - \beta)}, \quad x_A = \frac{2 - \bar{\alpha} - 2(\mu - r)}{1 - 2\bar{\alpha}},$$

corresponding to ZC_0/S and S/ZC_1 phase, respectively.

To analyze the behavior of the shock in the ZC_0/S phase, we fix $\mu = 0.4$ and $\alpha = 2$ and systematically vary the exit rate β . In Fig. 4, we present density profiles, shock position, and shock height for different values of β , providing a visual representation of the shock's dynamics. The observation reveals that with increasing β , the shock moves from the left towards the right and eventually reaches the left boundary of lane B, as depicted in Fig. 4. Furthermore, the shock height decreases linearly with respect to β . The corresponding value of height of the shock is $\Delta = 1 - \beta - \alpha_{\text{eff}} = 1 - 2\beta$ and maintains a positive value as x_B approaches 0. This phenomenon suggests the existence of a tanh-type boundary layer at the left end, signifying a transition from the ZC_0/S phase to the ZC_0/HD phase. Physically, this can be understood as follows. When $\beta = 0$, signifying a zero exit rate, particles tend to accumulate near the right end of lane B. As a result, the particle number in the reservoir increases, ultimately enhancing the effective entry rate. Consequently, the particle density at the left end rises while at the right end, it decreases, resulting in a reduction in the height of the shock.

Conversely, in investigating the propagation of the shock with fixed $\mu = 0.4$ and $\beta = 0.2$, while varying α , it is noted that the rapid movement of x_A inversely correlates with α , causing the shock height to shift swiftly from 1 to 0 (see

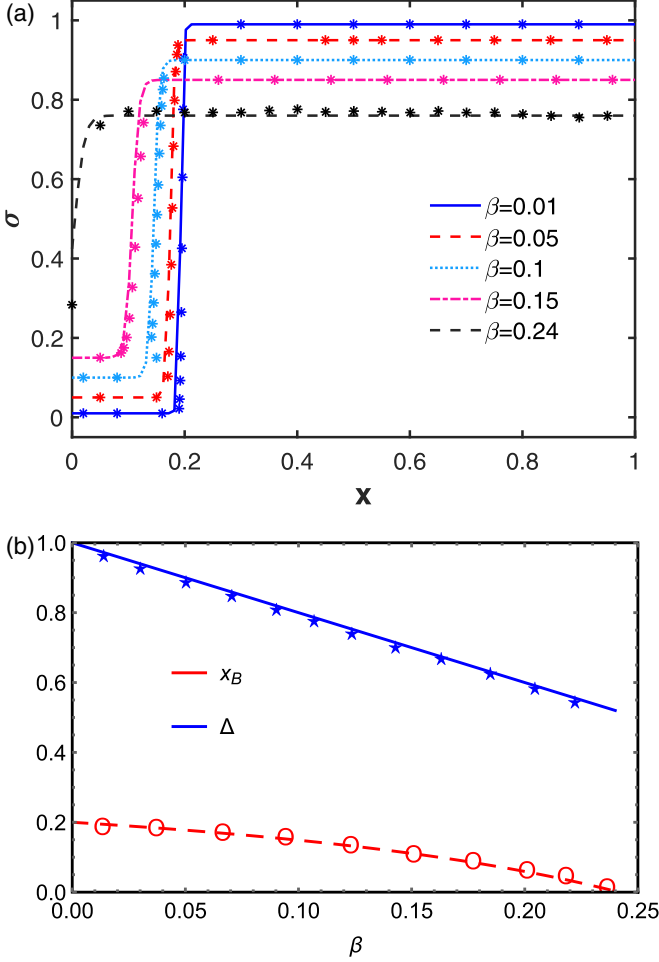


FIG. 4. (a) Density profiles of particles in lane A with $\alpha = 2$, $\mu = 0.4$ and $\beta = 0.01, 0.05, 0.1, 0.15$, and $\beta = 0.24$. (b) Position and height of the shock in ZC_0/S phase with respect to β for fixed $\alpha = 2$ and $\mu = 0.4$. The variable $\Delta = 1 - \beta - \alpha_{\text{eff}}$ gives the height of the shock. Symbols describe Monte Carlo results, while solid, dashed, and dotted lines correspond to theoretical findings.

Fig. 5). Meanwhile, the shock height maintains a steady value of $1 - 2\beta$.

Comparable analyses can be employed to investigate the S/ZC_1 phase. When (μ, β) is fixed at $(0.9, 0.1)$, the shock consistently moves towards the left and its height stabilizes at a constant value of $-\beta + \sqrt{1 - 6\beta + \beta^2}$ which can be computed by utilizing Eq. (45).

2. Downward synchronized shock

Now we explore the shock dynamics for the phases involving synchronized shocks in both lanes. Employing $\mu = 1$ and $\beta = 0.4$, we continuously increase the entry rate of the particles (refer to Fig. 6). The position and the height of the shock in this category is given by

$$x_s = \frac{2(\mu - r) - (1 - \beta)}{2\beta}, \quad \Delta = \beta. \quad (56)$$

The system enters this phase at $\alpha \approx 0.58$ just before which the system manifests the ZC_0/HD phase. As the value of α increases, the position of the boundary layer starts shift-

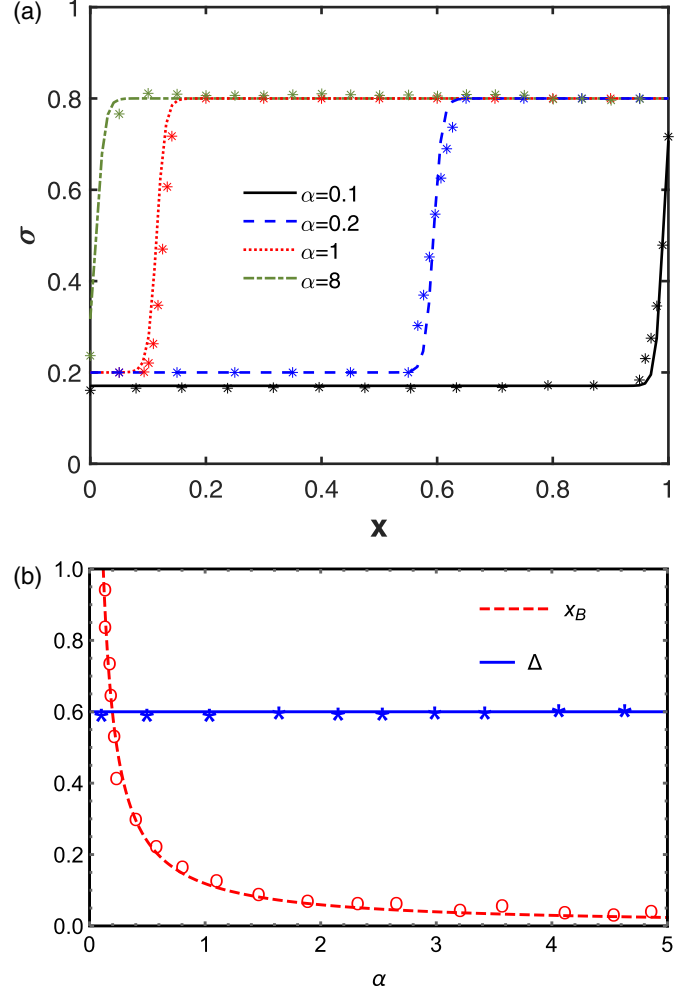


FIG. 5. (a) Density profiles of particles in lane A with $\beta = 0.2$, $\mu = 0.4$ and $\alpha = 0.1, 0.2, 1$, and $\beta = 8$. (b) Position and height of the shock in ZC_0/S phase with respect to α for fixed $\beta = 0.2$ and $\mu = 0.4$. The variable $\Delta = 1 - \beta - \alpha_{\text{eff}}$ gives the height of the shock. Symbols describe Monte Carlo results, while solid, dashed, and dotted lines correspond to theoretical findings.

ing from the left end of the lanes to enter the bulk of both the lanes and thus the system exhibits the $LD-ZC_0/ZC_1$ -HD phase constituting a downward shock in each lane. At the critical value of $\alpha \approx 1.34$, this downward shock reaches the right end of the lanes and the system transitions into LD/ZC_1 phase. However, no change in the height of the shock occurs; finally, a boundary layer of coth-type is detected in LD/ZC_1 for both lanes. From the above analysis, one can conclude that a second-order transition occurs from the ZC_0/HD to $LD-ZC_0/ZC_1$ -HD to LD/ZC_1 phase if one considers particle density as the order parameter.

On investigation of the other scenario, i.e., fixing $\alpha = 0.8$, and changing β , we observe a continuous phase transition from the $LD-ZC_0/ZC_1$ -HD phase to the $MC-ZC_0/ZC_1$ -MC phase as shown in Fig. 7. At $(\alpha, \beta) = (0.8, 0.28)$, the system is in LD/ZC_1 . If one monitors the position and the height of the shock, then they monotonically decrease and increase, respectively, with an increasing exit rate up to $\beta = 0.5$. Both of these values saturate at the point $\Delta = 0.5$, thus violating the

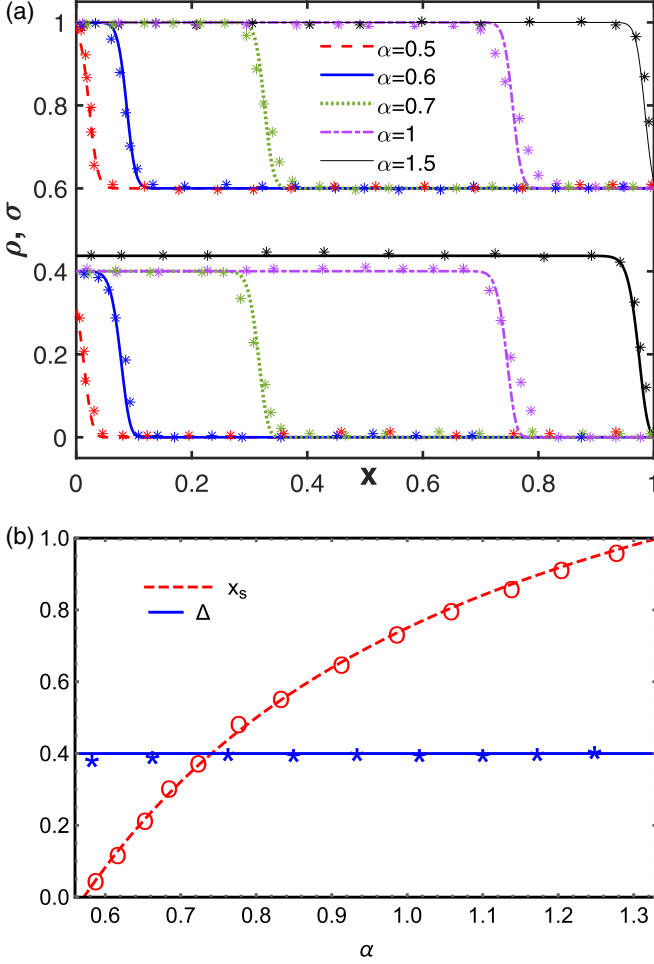


FIG. 6. (a) Density profile and (b) position as well as the height of the shock in LD-ZC₀/ZC₁-HD phase for fixed $(\mu, \beta) = (1, 0.4)$. The variable $\Delta = \beta$ gives the height of the shock. Symbols describe Monte Carlo results, while solid and dashed lines correspond to theoretical findings.

condition of existence of the LD-ZC₀/ZC₁-HD phase. So the system transitions into MC-ZC₀/ZC₁-MC phase indicating a second-order continuous transition.

VII. SUMMARY AND CONCLUSION

To summarize, we offer a thorough overview of two totally asymmetric simple exclusion lanes: one characterized by particle detachment and the other by particle attachment. In particular, the particles of a specific lane are compelled to move vertically once the corresponding vertical site becomes vacant. If this vertical movement is not feasible, then they simply pursue horizontal motion along their designated lane. Investigation of this interconnected system occurs within a constrained resource setting, where the filling factor defines the number of particles in the system. This restriction influences the entry rate of particles into the lanes.

The particle movement relies significantly on the vertical site in the adjacent lane, so we employ the vertical cluster mean-field technique to establish a theoretical framework. This approach aids in deriving explicit expressions for the

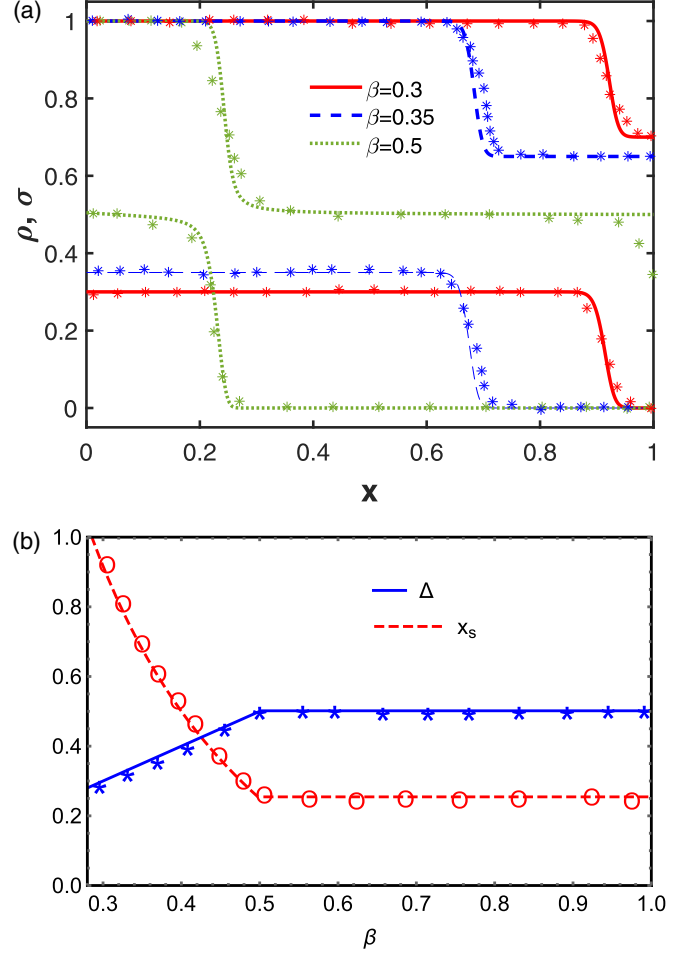


FIG. 7. (a) Density profile and (b) position as well as the height of the shock in the LD-ZC₀/ZC₁-HD phase for fixed $(\mu, \alpha) = (1, 0.8)$ and different values of β . The variable Δ gives the height of the shock. Symbols describe Monte Carlo results, while solid and dashed lines correspond to theoretical findings.

bulk stationary properties of each lane. However, to thoroughly analyze the system, we utilize singular perturbation theory to explore the stationary properties of the system in detail. To corroborate our analytical findings, we conduct kinetic Monte Carlo simulations (equivalent to the Gillespie algorithm) for validation, complemented by a numerical approach involving a finite-difference scheme applied to the continuum version of the system.

By employing a combination of analytical and numerical methods, we investigate the influence of limited particle resources on critical stationary properties of the system, including phase diagrams, particle densities, and phase transitions. Our analysis reveals two types of stationary phases: (i) one lane displays zero particle density, while (ii) the other lane exhibits maximum particle density, each implying no particle flow. The phase diagram undergoes notable qualitative and quantitative changes as the particle count in the system varies. Initially less complex, the phase diagram becomes more intricate with an intermediate particle count, eventually settling again into a simpler form. Specifically, the number of phases transitions from 2 to 6 to 8 to 10, where it reaches

its maximum before decreasing to 7 in the case of infinite particle resources. This implies that the number of phases that can persist follows a nonmonotonic trend with increasing particles in the system. Each phase diagram exhibits both bulk and surface transitions, the latter arising from the presence of a boundary layer in the system. Precisely, two types of surface transitions, \tanh and \coth , are observed in the system.

A salient feature of our study is the manifestation of both upward and downward shock in the system. The bulk solution to the left of an upward shock exhibits a smaller magnitude compared to the bulk solution on the right side. Conversely, in the scenario of a downward shock, this trend is reversed. The system manifests two phases marked by an upward shock and two phases defined by a downward shock. Under a specific set of parameters, the upward shock is localized to one lane within the system. Conversely, in the case of a downward shock, both lanes experience this phenomenon, and the shocks in both lanes are synchronized. We analyze the propagation of shocks concerning changes in both entrance and exit rates,

aiming for a comprehensive understanding of the phase transitions occurring in the system.

The main objective of this proposed work is to reveal the nonequilibrium stationary properties inherent in a two-lane coupled system operating under constrained conditions. By thoroughly investigating this system, we aim to shed light on the intricate dynamics governing diverse biological and physical transport processes. We expect that the insights gained from this study will not only advance our comprehension of these complex phenomena but will also establish a basis for future exploration in the broader field of nonequilibrium systems, potentially impacting various scientific disciplines.

ACKNOWLEDGMENT

The first author thanks the Council of Scientific & Industrial Research (CSIR), India, for financial support under File No: 09/1005(0023)/2018-EMR-I.

-
- [1] D. Chowdhury, L. Santen, and A. Schadschneider, Statistical physics of vehicular traffic and some related systems, *Phys. Rep.* **329**, 199 (2000).
 - [2] S. Klumpp and R. Lipowsky, Traffic of molecular motors through tube-like compartments, *J. Stat. Phys.* **113**, 233 (2003).
 - [3] K. Nagel, Particle hopping models and traffic flow theory, *Phys. Rev. E* **53**, 4655 (1996).
 - [4] T. Chou and G. Lakatos, Clustered bottlenecks in mrna translation and protein synthesis, *Phys. Rev. Lett.* **93**, 198101 (2004).
 - [5] B. Alberts, A. Johnson, P. Walter, J. Lewis, M. Raff, and K. Roberts, *Molecular Cell Biology* (Garland Science, New York, 2008).
 - [6] C. Appert-Rolland, M. Ebbinghaus, and L. Santen, Intracellular transport driven by cytoskeletal motors: General mechanisms and defects, *Phys. Rep.* **593**, 1 (2015).
 - [7] M. Schreckenberg, A. Schadschneider, K. Nagel, and N. Ito, Discrete stochastic models for traffic flow, *Phys. Rev. E* **51**, 2939 (1995).
 - [8] V. Belitsky, J. Krug, E. J. Neves, and G. M. Schütz, A cellular automaton model for two-lane traffic, *J. Stat. Phys.* **103**, 945 (2001).
 - [9] C. T. MacDonald, J. H. Gibbs, and A. C. Pipkin, Kinetics of biopolymerization on nucleic acid templates, *Biopolymers* **6**, 1 (1968).
 - [10] C. T. MacDonald and J. H. Gibbs, Concerning the kinetics of polypeptide synthesis on polyribosomes, *Biopolymers* **7**, 707 (1969).
 - [11] V. Popkov and G. M. Schütz, Steady-state selection in driven diffusive systems with open boundaries, *EPL* **48**, 257 (1999).
 - [12] J. Krug, Phase separation in disordered exclusion models, *Braz. J. Phys.* **30**, 97 (2000).
 - [13] A. B. Kolomeisky, G. M. Schütz, E. B. Kolomeisky, and J. P. Straley, Phase diagram of one-dimensional driven lattice gases with open boundaries, *J. Phys. A: Math. Gen.* **31**, 6911 (1998).
 - [14] B. Derrida, E. Domany, and D. Mukamel, An exact solution of a one-dimensional asymmetric exclusion model with open boundaries, *J. Stat. Phys.* **69**, 667 (1992).
 - [15] B. Derrida, M. R. Evans, V. Hakim, and V. Pasquier, Exact solution of a 1d asymmetric exclusion model using a matrix formulation, *J. Phys. A: Math. Gen.* **26**, 1493 (1993).
 - [16] B. Derrida and M. R. Evans, The asymmetric exclusion model: Exact results through a matrix approach, *Nonequilibrium Statistical Mechanics in One Dimension* (Cambridge University Press, Cambridge, UK, 1997), pp. 277–304.
 - [17] G. Schütz and E. Domany, Phase transitions in an exactly soluble one-dimensional exclusion process, *J. Stat. Phys.* **72**, 277 (1993).
 - [18] M. R. Evans, D. P. Foster, C. Godrèche, and D. Mukamel, Spontaneous symmetry breaking in a one dimensional driven diffusive system, *Phys. Rev. Lett.* **74**, 208 (1995).
 - [19] A. Miron and S. Reuveni, Diffusion with local resetting and exclusion, *Phys. Rev. Res.* **3**, L012023 (2021).
 - [20] R. J. Harris and R. B. Stinchcombe, Ideal and disordered two-lane traffic models, *Physica A* **354**, 582 (2005).
 - [21] T. Reichenbach, E. Frey, and T. Franosch, Traffic jams induced by rare switching events in two-lane transport, *New J. Phys.* **9**, 159 (2007).
 - [22] S. Xiao, X. Chen, L. Qi, and Y. Liu, *Totally asymmetric simple exclusion process with two consecutive ramps*, in *Journal of Physics: Conference Series*, Vol. 1324 (IOP Publishing, 2019), p. 012059.
 - [23] A. Gupta and A. K. Gupta, Reservoir crowding in a dynamically disordered bidirectional system with narrow entrances, *Chaos Solitons Fract.* **178**, 114318 (2024).
 - [24] D. Chowdhury, A. Garai, and J.-S. Wang, Traffic of single-headed motor proteins KIF1A: Effects of lane changing, *Phys. Rev. E* **77**, 050902(R) (2008).

- [25] S. Pradhan, S. Patra, Y. E. Dai, A. Schadschneider, and D. Chowdhury, Flux-density relation for traffic of army ants in a 3-lane bi-directional trail, *Physica A* **567**, 125664 (2021).
- [26] E. Pronina and A. B. Kolomeisky, Asymmetric coupling in two-channel simple exclusion processes, *Physica A* **372**, 12 (2006).
- [27] E. Pronina and A. B. Kolomeisky, Two-channel totally asymmetric simple exclusion processes, *J. Phys. A: Math. Gen.* **37**, 9907 (2004).
- [28] Q.-H. Shi, R. Jiang, M.-B. Hu, and Q.-S. Wu, Strong asymmetric coupling of two parallel exclusion processes, *J. Stat. Phys.* **142**, 616 (2011).
- [29] K. Tsekouras and A. B. Kolomeisky, Parallel coupling of symmetric and asymmetric exclusion processes, *J. Phys. A: Math. Theor.* **41**, 465001 (2008).
- [30] A. K. Gupta and I. Dhiman, Coupling of two asymmetric exclusion processes with open boundaries, *Physica A* **392**, 6314 (2013).
- [31] S. Xiao, P. Dong, Y. Zhang, and Y. Liu, Strong asymmetric coupling of two parallel exclusion processes: Effect of unequal injection rates, *Int. J. Theor. Phys.* **55**, 1642 (2016).
- [32] R. Jiang, M.-B. Hu, Y.-H. Wu, and Q.-S. Wu, Weak and strong coupling in a two-lane asymmetric exclusion process, *Phys. Rev. E* **77**, 041128 (2008).
- [33] A. Goswami, U. Dey, and S. Mukherjee, Nonequilibrium steadystates in coupled asymmetric and symmetric exclusion processes, *Phys. Rev. E* **108**, 054122 (2023).
- [34] Q.-H. Shi, R. Jiang, M.-B. Hu, and Q.-S. Wu, Strong asymmetric coupling of multilane pasesps, *Phys. Lett. A* **376**, 2640.
- [35] Z.-P. Cai, Y.-M. Yuan, R. Jiang, M.-B. Hu, Q.-S. Wu, and Y.-H. Wu, Asymmetric coupling in multi-channel simple exclusion processes, *J. Stat. Mech.: Theory Exp.* (2008) P07016.
- [36] R. Jiang, M.-B. Hu, K. Nishinari, R. Wang, and Q.-S. Wu, Shock formation in the periodic exclusion process with asymmetric coupling, *J. Stat. Mech.: Theory Exp.* (2010) P07003.
- [37] A. K. Verma and A. K. Gupta, Limited resources in multi-lane stochastic transport system, *J. Phys. Commun.* **2**, 045020 (2018).
- [38] S. Tamizhazhagan and A. K. Verma, Role of extended coupling in bidirectional transport system, *Phys. Rev. E* **106**, 014120 (2022).
- [39] S. Tamizhazhagan and A. K. Verma, Multiple reentrance transitions in exclusion process with finite reservoir, *Phys. Rev. E* **107**, 044133 (2023).
- [40] N. C. Priyanka and A. K. Verma, Asymmetric coupling inducestwo-directional reentrance transition in three-lane exclusion process, *Phys. Rev. E* **107**, 044104 (2023).
- [41] I. Dhiman and A. K. Gupta, Effect of coupling strength on a two-lane partially asymmetric coupled totally asymmetric simple exclusion process with langmuir kinetics, *Phys. Rev. E* **90**, 012114 (2014).
- [42] A. K. Gupta and I. Dhiman, Asymmetric coupling in two-lane simple exclusion processes with langmuir kinetics: Phase diagrams and boundary layers, *Phys. Rev. E* **89**, 022131 (2014).
- [43] I. Dhiman and A. K. Gupta, Collective dynamics of an inhomogeneous two-channel exclusion process: Theory and Monte Carlo simulations, *J. Comput. Phys.* **309**, 227 (2016).
- [44] S. Kukida, J. Tanimoto, and A. Hagishima, Analysis of the influence of lane changing on traffic-flow dynamics based on the cellular automaton model, *Int. J. Mod. Phys. C* **22**, 271 (2011).
- [45] S. Masukura, T. Nagatani, and K. Tanaka, Jamming transitions induced by a slow vehicle in traffic flow on a multi-lane highway, *J. Stat. Mech.: Theory Exp.* (2009) P04002.
- [46] A. Yamauchi, J. Tanimoto, A. Hagishima, and H. Sagara, Dilemma game structure observed in traffic flow at a 2-to-1 lane junction, *Phys. Rev. E* **79**, 036104 (2009).
- [47] N. Moussa, Simon–Gutowitz bidirectional traffic model revisited, *Phys. Lett. A* **372**, 6701 (2008).
- [48] K. Tanaka, T. Nagatani, and S. Masukura, Fundamental diagram in traffic flow of mixed vehicles on multi-lane highway, *Physica A* **387**, 5583 (2008).
- [49] P. Greulich, L. Ciandrini, R. J. Allen, and M. C. Romano, Mixed population of competing totally asymmetric simple exclusion processes with a shared reservoir of particles, *Phys. Rev. E* **85**, 011142 (2012).
- [50] L. J. Cook, R. K. P. Zia, and B. Schmittmann, Competition between multiple totally asymmetric simple exclusion processes for a finite pool of resources, *Phys. Rev. E* **80**, 031142 (2009).
- [51] T. L. Blasius, N. Reed, B. M. Slepchenko, and K. J. Verhey, Recycling of kinesin-1 motors by diffusion after transport, *PLoS One* **8**, e76081 (2013).
- [52] L. Ciandrini, I. Neri, J. C. Walter, O. Dauloudet, and A. Parmeggiani, Motor protein traffic regulation by supply–demand balance of resources, *Phys. Biol.* **11**, 056006 (2014).
- [53] A. Gupta, B. Pal, and A. K. Gupta, Interplay of reservoirs in a bidirectional system, *Phys. Rev. E* **107**, 034103 (2023).
- [54] N. Bhatia and A. K. Gupta, Far from equilibrium transport on tasep with pockets, *Eur. Phys. J. Plus* **137**, 892 (2022).
- [55] D. ben-Avraham and J. Köhler, Mean-field (n, m) -cluster approximation for lattice models, *Phys. Rev. A* **45**, 8358 (1992).
- [56] J. D. Cole and L. E. Levine, Perturbation methods in applied-mathematics (Springer, New York, 1981), Vol. 34.
- [57] S. Mukherji and V. Mishra, Bulk and surface transitions in asymmetric simple exclusion process: Impact on boundary layers, *Phys. Rev. E* **74**, 011116 (2006).